Research Article

Tiejun Li, Yue Sun, Weiren Shi, Guifang Shao, and Jianjun Liu*

Terahertz pulse imaging: A novel denoising method by combing the ant colony algorithm with the compressive sensing

https://doi.org/10.1515/phys-2018-0080
Received Dec 08, 2017; accepted Aug 07, 2018

Abstract: Terahertz (THz) pulse imaging exhibits a potential application in biomedicine, nondestructive detection and safety inspection. However, the THz time-domain spectroscopy system will affect the THz image quality. To improve the THz image quality, in this article we proposed a novel method by combining the ant colony algorithm with the compressive sensing method. First, the image edge is detected by using the ant colony algorithm. Subsequently, the compressive sensing method based on signal sparse representation and the reconstruction algorithm from partial Fourier is applied on the non-edge image for noise reduction. Finally, the reconstruction result is obtained by combining the noise reduced non-edge image with the edge image. The experimental results on three kinds of images prove that the proposed method can preserve the edge information during noise reduction.

Keywords: THz pulse imaging; ant colony algorithm; compressive sensing; denoising

PACS: 07.05.Pj, 07.05.Tp

1 Introduction

Terahertz is an electromagnetic wave with the frequency ranging from 0.1 to 10 THz, corresponding to a wavelength range of 30 μm to 3 mm. Terahertz pulse imaging (TPI), which is based on the electromagnetic radiation of THz wave, has appeared in the past decade [1]. TPI is a non-invasive coherent optical image modality, and has aroused widespread concerns owing to its potential applications in biomedical, trace gas analysis, nondestructive imaging of packages, inspection of artworks, counterfeit note, and semiconductor device diagnostics [2–5]. Generally, THz imaging technology includes coherent imaging and non-coherent imaging. The former typically contains time-domain spectroscopy imaging, electro optics imaging and chromatography imaging, yet continuous wave imaging usually belongs to the latter [6, 7]. To date, TPI investigation mainly involves two aspects. On one hand, a majority of researchers focuses on how to overcome the obstacles in hardware, that is, how to improve the resolution, accuracy and speed in TPI system [8–10]. On the other hand, few digital image processing methods have been introduced into further improvement of the quality of images obtained from the THz system [1, 11, 12].

Sometimes, the images obtained by the THz technique are not clear enough to distinguish their profile from the edge. Meanwhile, the THz images are usually affected by speckle noises, which will lower the target recognition accuracy. Therefore, the denoising becomes a key during THz image processing. However, the classical digital image denoising methods such as mean filter, median filter and non-local means (NLM) [13], will blur the image edge when reducing the noises. Therefore, to develop an effective denoising method is significant for the theoretical study of THz images.

Recently, the fourth-order partial differential equation (PDE) method has been introduced into image denoising study [14], displaying a good trade-off between noise removal and edge preservation. Furthermore, the ant colony algorithm (ACA) outperforms some traditional edge detection operators in image edge detection [15, 16]. The ACA is a swarm-based meta-heuristic method by simulating the natural foraging behavior of ant colonies. During image edge detection, a great quantity of ants is drove by the local intensity deviation to move on images, so as to establish a

***Corresponding Author: Jianjun Liu:** College of Food Science, Southwest University, Chongqing 400715, China; Email: king.jju.edu@outlook.com
Tiejun Li: School of Automation, Chongqing University, Chongqing 400044, China; Information Engineering College, Jimei University, Xiamen 361021, China
Yue Sun, Weiren Shi: School of Automation, Chongqing University, Chongqing 400044, China
Guifang Shao: Department of Automation, Xiamen University, Xiamen 361005, China

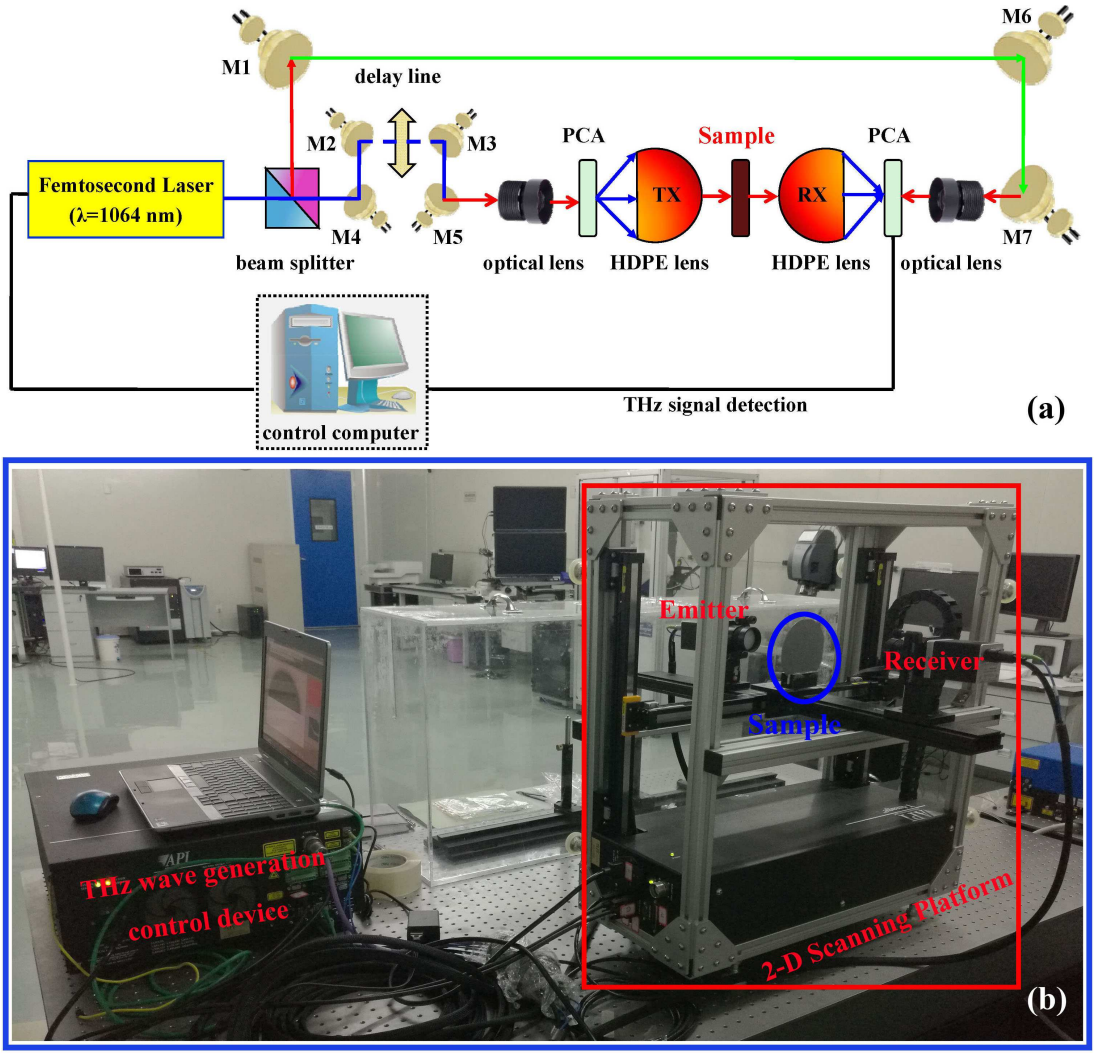

Figure 1: The schematic illustration of API T-Ray 5000 THz time domain spectrum transmission detection system with (a) diagram and (b) real system

pheromone matrix of edge information per pixel [17]. We also proposed a denoising method for THz images by combining the ACA and the adaptive threshold [1]. In addition, the compressive sensing (CS) theory has also attracted increasing attention in image denoising [18, 19].

Based on the pioneering studies mentioned above, to maintain the edge information during noise removal, here we propose a new method by combining the ACA and the CS method. First, the ACA is used to detect the image edge. Secondly, a pheromone matrix is constructed by numerous ants moving on a 2-D image. Thirdly, the CS method is applied to reduce the noises on non-edge image. Meanwhile, the reconstruction algorithm based on partial Fourier transform (RecPF) [18] is used for image reconstruction in the CS method. Finally, the denoising non-edge image and the edge image are combined to reconstruct the final result. This article is organized as follows. Section 2 describes how to obtain the THz images through experimental apparatus. The ACA for edge detection and the CS denoising approach are presented in Section 3. The calculated results and the related discussion are presented in Section 4. The main conclusions are summarized in Section 5.

2 Experimental apparatus

In this article, a transmission time-domain spectroscopy detection system is used and the API T-Ray 5000 developed by Advanced Photonix Inc. is adopted for generating the THz image, as shown in Figure 1. Meanwhile, the femtosecond pulse laser is generated by a Titanium sap-

phire laser. Its central output wavelength is 1064 nm, the repetition frequency is 100 MHz, single pulse energy is 20 mW and pulse width is 80 fs. Then the photoconductive antenna (PCA) is adopted for generating and detecting the THz pulse. Subsequently, the laser beam, produced by the femtosecond laser, is divided into the pump light and the probe light by a cubic beam splitter (CBS) for THz generation and detection. In addition, the CCD camera, as a detector, can obtain the real-time optical image of sample. Finally, the measured sample is placed on the two-dimensional scanning step platform with the positional accuracy of 1 μm.

In addition, for the THz-time-domain spectroscopy system used in this article, its effective frequency bandwidth is 0~3.5 THz, the spectral resolution is 12.5 GHz, the fast scan range is 80 ps, the time resolution is 0.1 ps, the spot diameter is 1.2 m and its optical resolution is smaller than 0.5 mm. The actual API T-Ray 5000 system is displayed in Figure 1b. During the experiment, the THz wave emitter and receiver lens are fixed at the horizontal optical slide, and the sample is placed at the 2-D scanning platform, which can move in XY direction. Furthermore, the sample also lies on the focusing position of THz pulse, so we can realize the THz pulse imaging for sample by the 2-D scanning of stepping motor. For image scanning, the sample is exposed to dry air for detection, and the scanning step is set for 0.25 mm, the horizontal line scanning speed is 100 mm/s.

According to the aforementioned system, we may obtain a THz image by some imaging techniques based on the time domain waveform or frequency domain wave spectrum in THz electric field, such as the maximum value imaging or amplitude imaging of time domain, and maximum frequency spectrum imaging. However, the THz image quality will vary greatly because the different techniques extract diverse information of sample for imaging. What's more, the experimental environment and hardware performance will also introduce noises into the THz image background. For example, the sensitivity of detector, the low pass effect of aerial system and the diffraction effect of imaging system will cause obvious noises in THz images. Therefore, the image denoising is crucial for application of THz imaging in different fields.

3 Methodology

The edge information is vital for THz image processing. To preserve the edge information during denoising process, we proposed to combine the ACA and the CS. The edge detection is first conducted in THz image to obtain the edge image and non-edge image by using the ACA. Note that the ACA is referred to our previous work [1]. Furthermore, the CS method is applied in the non-edge image for noise removing. Finally, the noise removal image on non-edge is combined with the edge image to reconstruct the final denoising image, as shown in Figure 2.

3.1 Edge detection with ACA

Supposing a THz image I of size $H \times W$, and $I_{i,j}$ denotes the intensity value of the pixel at position (i, j). Let each pixel as a node, the edge detection with the ACA can be executed according to the following four steps: 1) initialization, 2) construction, 3) update, and 4) decision.

The details of the pseudo code are shown in Algorithm 1, as shown in Figure 3.

Step 1: At first, set each element of the pheromone matrix $\tau^{(0)}$ to constant τ_{init}.

Step 2: Secondly, choose one ant at random among the total S ants during the n-th construction step, and let it continuously move L movement-steps on the image according to an eight-connected neighborhood. For moving from node (l, m) to its neighbor node (i, j), a transition probability is defined by the following formula

$$p^{(n)}_{(l,m)(i,j)} = \frac{(\tau^{(n-1)}_{i,j})^{\alpha}(\eta_{i,j})^{\theta}}{\sum_{(i,j)\in\Omega_{(l,m)}}((\tau^{(n-1)}_{i,j})^{\alpha}(\eta_{i,j})^{\theta})} \tag{1}$$

where $\tau^{(n-1)}_{i,j}$ is the pheromone value of the node (i, j), and $\Omega_{(l,m)}$ represents the neighbor node set of the node (l, m). The impact of pheromone matrix and heuristic matrix are described by constants α and θ, respectively. The heuristic information of node (i, j) is denoted by $\eta_{i,j}$ and expressed as

$$\eta_{ij} = \frac{1}{Z}V_c(I_{i,j}) \tag{2}$$

in which, $Z = \sum_{i=1:M_1}\sum_{j=1:M_2}V_c(I_{i,j})$ is a normalization factor. The relationship of pixels c in local region (called the *clique*) can be described by a function $V_c(I_{i,j})$ and its value is decided by the intensity deviations of c. For example, it can be defined as

$$\begin{aligned} V_c(I_{i,j}) = f(&|I_{i-2,j-1} - I_{i+2,j+1}| \\ &+ |I_{i-2,j+1} - I_{i+2,j-1}| + |I_{i-1,j-2} - I_{i+1,j+2}| \\ &+ |I_{i-1,j-1} - I_{i+1,j+1}| + |I_{i-1,j} - I_{i+1,j}| \\ &+ |I_{i-1,j+1} - I_{i-1,j-1}| + |I_{i-1,j+2} - I_{i+1,j-2}| \\ &+ |I_{i,j-1} - I_{i,j+1}|) \end{aligned} \tag{3}$$

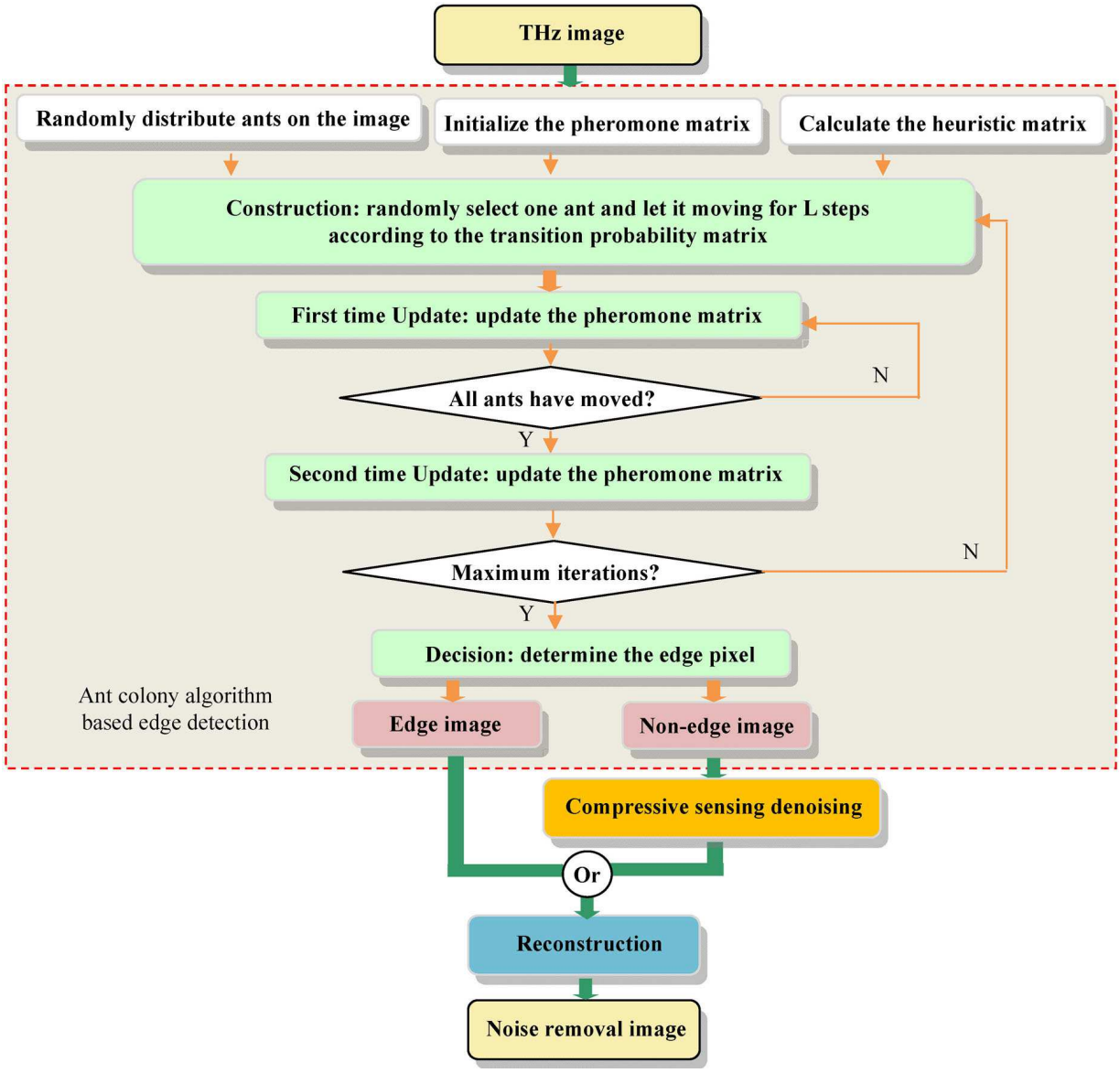

Figure 2: The diagram of the proposed method

Here we adopt a parameter σ to adjusts the functions' respective shapes and the function $f(\cdot)$ in Eq. (3) can be determined as

$$f(x) = \begin{cases} \frac{\pi x \sin(\frac{\pi x}{\sigma})}{\sigma} & 0 \le x \le \sigma; \\ 0 & else \end{cases}. \tag{4}$$

Step 3: Thirdly, two update operations are performed for the pheromone matrix. The first one is conducted when every ant finishes its movement during each construction step and given as

$$\tau_{i,j}^{(n-1)} = \begin{cases} (1-\rho)\tau_{i,j}^{(n-1)} + \rho\Delta_{i,j}^{(k)}, & otherwise. \\ \tau_{i,j}^{(n-1)}, & (i,j)\ is\ not\ visit\ by\ k^{th}\ ant \end{cases} \tag{5}$$

where ρ represents the evaporative rate, and $\Delta_{i,j}^{(k)}$ is decided by the heuristic matrix $\Delta_{i,j}^{(k)} = \eta_{i,j}$.

The other is performed while all ants complete their movements among every construction step and is defined as

$$\tau^{(n)} = (1-\psi)\cdot\tau^{(n-1)} + \psi\cdot\tau^{(0)} \tag{6}$$

in which, ψ denotes the pheromone decay coefficient.

Step 4: Then the ant movement operation has been run for S iterations in order to build the ultimate pheromone matrix $\tau^{(S)}$ by iteratively executing step 2 and step 3.

Step 5: Finally, to obtain the edge, a decision-making process based on threshold T is carried out according to the

Algorithm 1
The pseudo code of the ant colony algorithm

Input: M the total number of ants. S the total number of construction-steps.
α the weighting factor of the pheromone information.
θ the weighting factor of the heuristic information.
Ω the connectivity neighborhood. σ the adjusting factor.
τ_{init} the initial value of each component of the pheromone matrix.
ρ the evaporation rate. ψ the pheromone decay coefficient.
L total number of ant's movement-steps within each construction-step.
Output: Detect the image edge.
Initialize the pheromone matrix $\tau^{(0)} \leftarrow \tau_{init}$;
for $n \leftarrow 1$ **to** S **do**
  for $k \leftarrow 1$ **to** M **do**
    Randomly select one ant (k);
    Consecutively move the ant(k) for L steps according to Eq.(1);
    if position (i, j) is visited by ant(k)
      update the pheromone matrix $\tau^{(n)}$ based on Eq.(5);
    end
  end
  if all the ants have visited position (i, j)
    update the pheromone matrix $\tau^{(n)}$ based on Eq.(6);
  end
end
Adaptively compute the threshold T according to Eq.(7);
Make the solution decision with threshold T on the final pheromone matrix $\tau^{(S)}$;
return;

Figure 3: The pseudo code of the ACA

following equation

$$T^{(l)} = \frac{m_L^{(l)} + m_U^{(l)}}{2} \tag{7}$$

The threshold T can be gained by the following operations: Let the mean of $\tau^{(S)}$ as the initial threshold $T^{(0)}$ and divide $\tau^{(S)}$ into two classes by the criterion of lower or upper than $T^{(0)}$, then compute the new threshold based on Eq. (7) until its value maintains unchanged.

3.2 Denoising based on the CS algorithms

Recently, the CS algorithms are widely used in image denoising. In particular, the CS reconstruction algorithm based on the total variation regularization has attracted extensive interest due to the fact that it can preserve the essential characteristic information of image such as edge and texture. For example, Yang *et al.* proposed a novel image reconstruction algorithm, RecPF, based on local Fourier transform [18]. This algorithm can quickly resolve the image reconstruction problem by solving the minimized total variation method. In this paper, the aforementioned CS method is introduced to reduce the noise. Constructing a CS denoising model involves three steps: 1) the sparse representation of image signal, 2) the sensing measurement of signal, and 3) the RecPF based reconstruction algorithm for image restoration.

Step 1: The sparse representation of signal.

Supposing that image I with $N = H \times W$ pixels, the signal sparse representation is defined as follows:

$$I = \sum_{i=1}^{N} \psi_i x_i = \Psi x \tag{8}$$

where $\Psi = [\psi_1, \psi_2, \ldots\ldots \psi_N] \in R^{N\times N}$ represents the standard orthogonal basis of R^N and the Ψ is chose as wavelet orthogonal basis. $x \in R^N$ denotes the vector of inner product $x_i = \langle I, \psi_i \rangle$. $\|x\|_0 = K$, K is the nonzero numbers in vector x and $K << N$, then we can name I as the K sparse in Ψ domain.

Step 2: The sensing measurement of signal.

The essential part of the CS method is the linear measurement. The original image signal I can be measured by sampling it according to a linear measurement matrix Φ in size of $M \times N$, and $K < M << N$. The measurement vector $b \in R^M$, as M linear measurements of I, is given as follows

$$b = \Phi I \tag{9}$$

Substitute Eq. (8) into Eq. (9), we can obtain

$$b = \Phi I = Ax, \quad A = \Phi\psi \in R^{M\times N} \tag{10}$$

Here, A is called as the sensing measurement matrix and the measurement matrix Φ is defined by a local Fourier matrix, which satisfies the restricted isometry property. On the basis of the CS theory, the signal I can be reconstructed by the measurement vector $b = Ax$.

Step 3: The signal reconstruction algorithm based on RecPF.

First of all, the partial frequency observation f_p for image I is given by

$$f_p = F_p I + \omega \tag{11}$$

in which, $F_p \in C^{p\times N}$ represents a partial discrete Fourier transform and serves as a measurement matrix in the CS method. p is the row number of F_p and $\omega \in C^p$ denotes the random noises.

The RecPF algorithm reconstructs the image $\bar{I}$ from f_p and realizes it by solving the following TVL1-L2 model

$$\min_I \sum_i ||D_i\bar{I}||_2 + \tau||\Psi^T\bar{I}||_1 + \mu(1/2)\cdot||F_p\bar{I} - f_p||_2^2 \tag{12}$$

where D_i is a 2*N matrix, $D_i\bar{I}$ denotes the horizontal and vertical partial total variances of $\bar{I}$ under pixel i. $\sum_i ||D_i\bar{I}||_2$ represents the discretization of the total variance of $\bar{I}$. $||\Psi^T\bar{I}||_1$ defines the l_1 norm of $\bar{I}$ under wavelet basis Ψ. $\tau, \mu > 0$ are the balance regulation parameters.

Table 1: Parameter setting for edge detection method with the ACA

parameter	value	parameter	value	parameter	value	parameter	value	parameter	value
α	1	σ	1	ψ	0.05	Ω	8	τ_{init}	0.001
θ	0.1	ρ	0.1	S	4	L	40	M	$\sqrt{H \times W}$

Table 2: Parameter setting for the CS method

parameter	value	parameter	value	parameter	value	parameter	value	parameter	value
γ	1.618	μ	10^{-6}	β	2^5	δ	5	RLs	22
τ	1	p	6	r	9.36%	ε	10^{-3}		

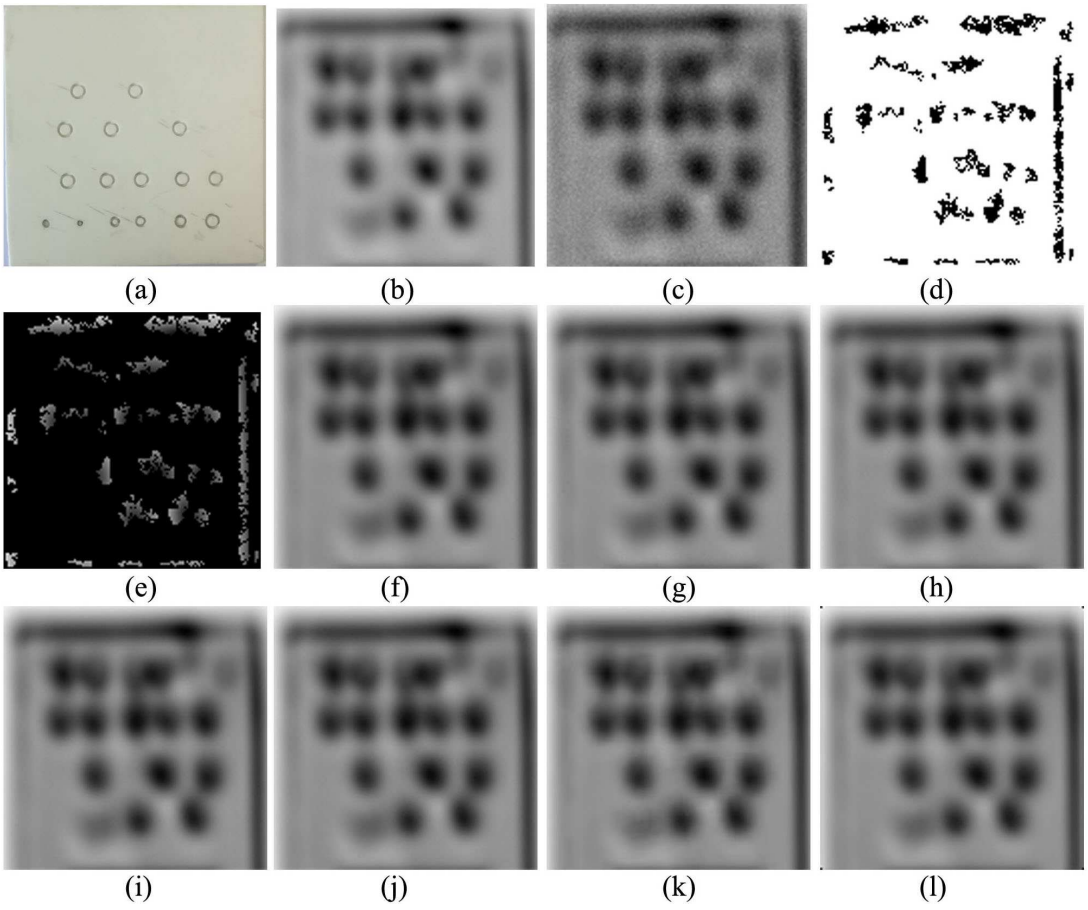

Figure 4: Denoising results of Al_2O_3 ceramic: (a) optical image; (b) THz image; (c) Noised THz image; (d) edge image; (e) non-edge image; denoised images by (f) Donoho threshold; (g) Generalized wavelet threshold; (h) fourth-order partial differential; (i) adaptive thresholding; (j) Bayes thresholding;(k) BM3D; (l) our proposed approach

The vital contribution of the RecPF algorithm is reformulated Eq. (12) into the following form

$$\min_{w,z,u} \sum_i ||w_i||_2 + \tau\|z\|_1 + \mu\theta(\bar{I}, f_p) \quad (13)$$
$$s.t. w_i = D_i\bar{I}, \forall i; z = \Psi^T\bar{I}.$$

in which, $z \in R^N$ and $\theta(\bar{I}, f_p) = (1/2) \cdot ||F_p\bar{I} - f_p||_2^2$.

4 Experiments

To conduct the experiments, the used THz images were obtained from the system introduced in Section 2. Three kinds of THz images, Al_2O_3 ceramic 128×128, plastic encapsulated IC chip 128×128, and solar panel 128×128, were adopted for comparison. At the same time, five differ-

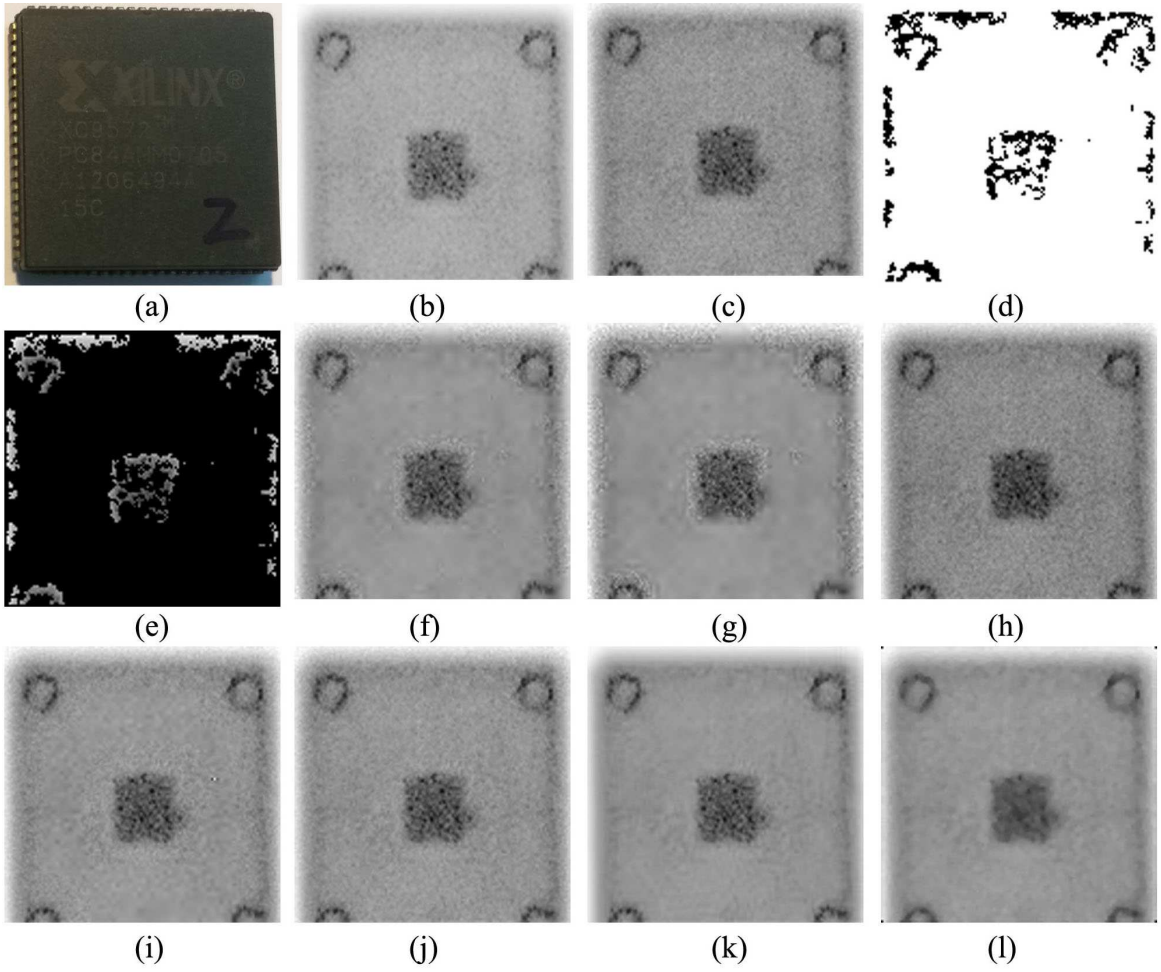

Figure 5: Various results of plastic encapsulated IC chip: (a) optical image; (b) THz image; (c) Noised THz image; (d) edge image; (e) non-edge image; denoised images by (f) Donoho threshold; (g) Generalized wavelet threshold; (h) fourth-order partial differential; (i) adaptive thresholding; (j) Bayes thresholding; (k) BM3D; (l) our proposed approach

ent methods, that is, Donoho Threshold [20], Generalized Wavelet Threshold [21], Adaptive thresholding [1], Four-order partial differential equations [14] and Bayes threshold [22], were selected for comparison. Furthermore, the block-matching and 3D filtering (BM3D) method [23] (www.cs.tut.fi/~foi/GCF-BM3D/) was applied for the original THz image denoising. These denoising methods were executed with the programming language of Matlab in version 2014a and run on the PC owning an i5-2400 processor with 3.1 GHz CPU and a 4096 MB RAM. One hundred experiments were conducted for each of the aforementioned approaches. In addition, the parameters involved in the proposed methods are given in Tables 1 and 2.

According to the number of central radiation lines in Fourier domain [18], the local fast Fourier transform sampling for image signal can be carried out. The number of radial lines RLs is proportional to the quantity of measurement vector. Therefore, we can define the sampling rate as $r{=}M/N$.

5 Results and discussion

First, the proposed method is compared with the other six approaches mentioned above on three different THz images. Figures 4-6 show the experimental results. It can be concluded that the Donoho threshold, the generalized wavelet threshold and the four-order partial differential method become worse, because they will lose some useful information. Specifically, the Donoho threshold and the generalized wavelet threshold will blur the image edge. In addition, the adaptive thresholding, the Bayes thresholding and the BM3D algorithms possess better denoising effects than the former three ones. Finally, our proposed ap-

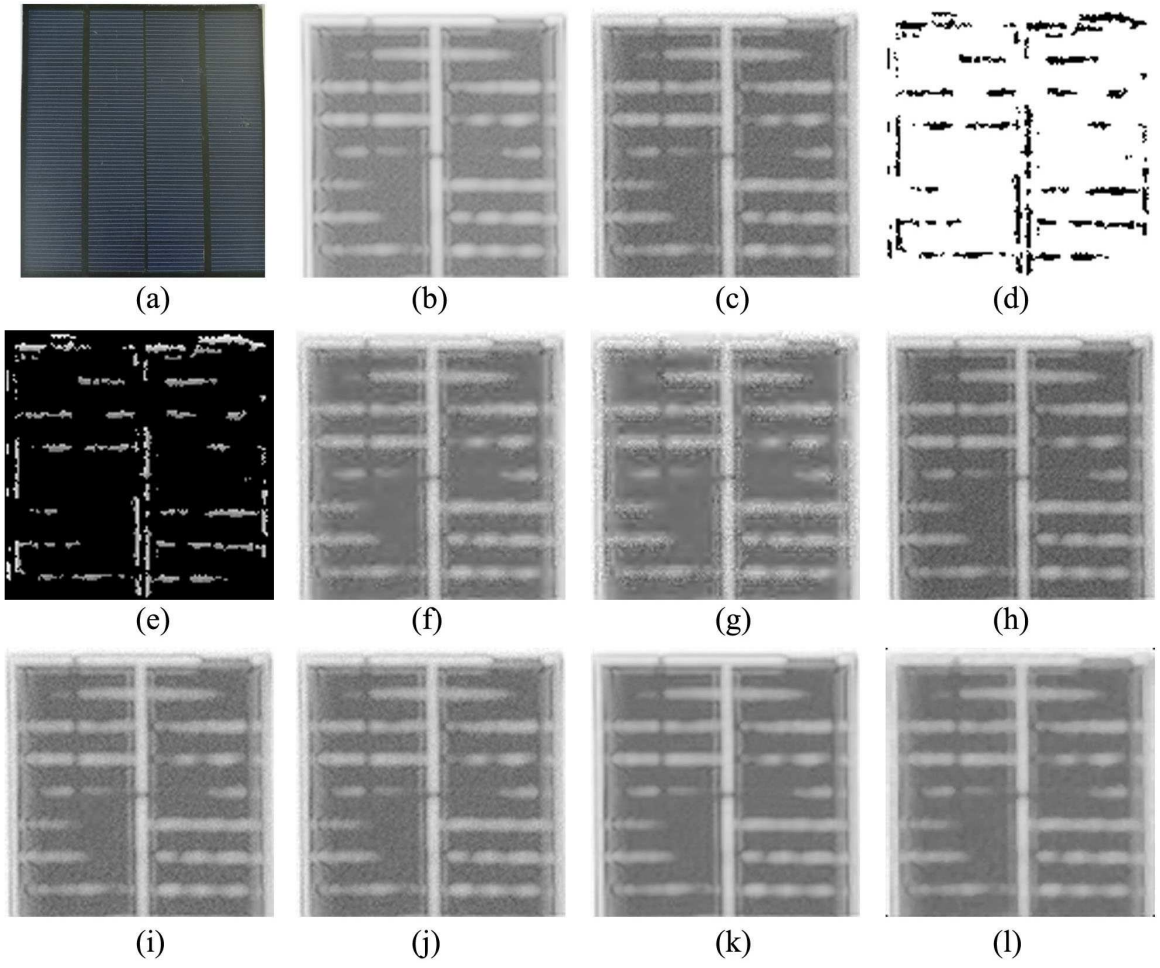

Figure 6: Various results of solar panel: (a) optical image; (b) THz image; (c) Noised THz image; (d) edge image; (e) non-edge image; denoised images by (f) Donoho threshold; (g) Generalized wavelet threshold; (h) fourth-order partial differential; (i) adaptive thresholding; (j) Bayes thresholding; (k) BM3D; (l) our proposed approach

proach exhibits better denoising results than all the other methods, as indicated in Figures 4-6.

Furthermore, the mean squared error (MSE), the signal-to-noise ratio (PSNR), the root mean square (RMS) and the normalized mean square error (NMSE) are explored on the denoising results by using these methods. Their definitions have been expressed as follows

$$MSE = \frac{1}{mn}\sum_{i=0}^{m-1}\sum_{j=0}^{n-1}||\bar{I}_{ij} - I_{ij}||^2 \tag{14}$$

$$PSNR = 10 \cdot \log_{10}\left(\frac{MAX^2}{MSE}\right)$$

$$RMS = \sqrt{\frac{1}{mn}\sum_{i=0}^{m-1}\sum_{j=0}^{n-1}||\bar{I}_{ij} - I_{ij}||^2}$$

$$NMSE = \frac{1}{sumx}\sum_{i=0}^{m-1}\sum_{j=0}^{n-1}||\bar{I}_{ij} - I_{ij}||^2$$

in which MAX is the largest value of image point, $sumx = \sum_{i=0}^{m-1}\sum_{j=0}^{n-1} {I_{ij}}^2$, and the unit of PSNR is dB. Their results have been summarized in Table 3. In addition, the computational complexity (run time) of the proposed approach compared with other six methods is also conducted, as shown in Table 3.

It can be seen from Table 3 that the MSE, the NMSE, and the RMS of our proposed approach are the smallest among all the methods, meaning that the denoised image has a little difference from the original image. More importantly, the PSNR of our proposed approach is the largest one among these seven models, indicating that our proposed method can preserve the edge information to a large extent during removing the noises. Furthermore, the processing time of our method is only a little larger than those of the other algorithms. Therefore, these experimental results reveal that our purposed method displays better per-

Table 3: The PSNR, MSE, NMSE, RMS and Run time performance comparison

Test image Al_2O_3 ceramic	PSNR(dB)	MSE	NMSE	RMS	Run time(s)
Donoho	50.4104	7.9802e–06	1.7273e–05	2.8249e–03	0.087198
Generalized wavelet	48.7003	1.1945e–05	2.5856e–05	3.4562e–03	0.105893
Fourth-order partial differential	33.4624	3.9250e–04	8.4982e–04	1.9812e–02	0.356542
Adaptive thresholding	65.1793	2.6431e–07	5.7211e–07	5.1411e–04	0.334712
Bayes	59.2316	1.0392e–06	2.2493e–06	1.0194e–03	0.045632
BM3D	35.3052	4.2424e–05	9.1828e–05	6.5134e–03	0.193258
Our proposed approach	121.8691	5.6646e–13	1.2261e–12	7.5263e–07	1.708356
Test image plastic encapsulated IC chip	PSNR(dB)	MSE	NMSE	RMS	Run time(s)
Donoho	31.8385	6.5570e–04	1.1370e–03	2.5607e–02	0.317337
Generalized wavelet	30.2222	1. 0881e–03	1. 8868e–03	3.2987e–02	0.139210
Fourth-order partial differential	17.8287	1.6487e–02	2.8588e–02	1.2840e–01	0.349308
Adaptive thresholding	37.5001	1.7774e–04	3.0820e–04	1.3332e–02	0.348671
Bayes	43.8690	4.0805e–05	7.0757e–05	6.3878e–03	0. 055943
BM3D	37.3998	3.0048e–04	5.2105e–04	1.7334e–02	0. 349877
Our proposed approach	115.1775	3.0356e–12	5.2639e–12	1.7423e–06	0.928969
Test image solar panel	PSNR(dB)	MSE	NMSE	RMS	Run time(s)
Donoho	32.0230	6.8164e–04	1. 1914e–03	2.6108e–02	0.332466
Generalized wavelet	29.2622	1. 3800e–03	2.4121e–03	3.7149e–02	0.136761
Fourth-order partial differential	18.0187	1.5781e–02	2. 7582e–02	1.2562e–01	0.345670
Adaptive thresholding	44. 2010	3.8474e–05	6.7247e–05	6.2028e–03	0.335675
Bayes	41. 1995	7.8005e–05	1.3634e–04	8.8320e–03	0.053507
BM3D	38.1335	2.7892e–04	4.8746e–04	1.6701e–02	0.302251
Our proposed approach	115.9573	2.5367e–12	4.4337e–12	1.5927e–06	0.919647

formance in THz image denoising than the other six methods.

6 Conclusions

The THz pulse imaging has attracted great interest on biomedicine, measurement and detection. However, background noises may sometimes exist in THz images due to the influence of THz pulse coherent superposition in detector. In this paper, we propose a novel method by combining the ant colony algorithm (ACA) and the compressive sensing (CS) method to enhance the image quality. The experiments on three different THz images reveal that our proposed method can largely reduce noises and preserve the edge information compared with six methods available. Furthermore, the PSNR of our proposed method on three different THz images are nearly 3 to 5 times that of the six algorithms. In addition, the processing time of the proposed method is a little longer than the other approaches due to its complexity.

Acknowledgement: This work is supported by the National Natural Science Foundation of China (Grant Nos. 61403318 and 61304141), the Fundamental Research Funds for the Central Universities of China (Grant No. 20720160085), the Guangxi Key Laboratory of Automatic Detecting Technology and Instruments (No. YQ17204), the Key Science and Technology of Jiangxi Education Department (No. GJJ161067), the State Key Development Program for Basic Research of Health and Family Planning Commission of Jiangxi Province China (No. 20175560), the China Postdoctoral Science Foundation Funded Project on the 61th Grant Program (No. 2017M610581).

References

[1] Liu J.J., Li Z., Ant colony combined with adaptive threshold denoising and reconstruct for THz image, Optik, Int. J. Light Electr. Optics, 2014, 125(14), 3423-3427.

[2] Lin H.Y., Dong Y., Shen Y.C. and Zeitler J.A., Quantifying pharmaceutical film coating with optical coherence tomography and terahertz pulsed imaging: an evaluation, J. Pharm. Sci., 2015, 104(10), 3377-3385.

[3] Jolly A., Gokhan F.S., Jolly J.C., Hocquet S. and Chassagne B., Combination of silicon phase masks with time-domain spectroscopy for single-scan terahertz imaging, Appl. Phys. B-Lasers. O, 2015, 120(3), 441-450.

[4] Jackson J.B., Labaune J., Bailleul L.R., Alessandro L.D., Whyte A., Bowen J.W., Menu M. and Mourou G., Terahertz pulse imaging in archaeology, Front. Optoelectron, 2015, 8(1), 81-92.

[5] Yassin S., Su K., Gladden L.F. and Zeitler J.A., Diffusion and swelling measurements in pharmaceutical powder compacts using terahertz pulsed imaging, J. Pharm. Sci., 2015, 104(5), 1658-1667.

[6] Obradovic J., Collins J.H.P., Hirsch O., Mantle L.D., Johns M.L. and Gladden L.F., The use of THz time-domain reflection measurements to investigate solvent diffusion in polymers, Polymer, 2007, 48(12), 3494-3503.

[7] Sun W.F., Wang X.K. and Zhang Y., Continuous wave terahertz phase imaging with three-step phase-shifting, Optik-International Journal for Light and Electron Optics, 2013, 124(22), 5533.

[8] Chen H.T., Kersting R. and Cho G.C., Terahertz imaging with nanometer resolution, Appl. Phys. Lett., 2003, 83(15), 3009-3011.

[9] Shon C.H., Chong W.Y., Jeon S.G., Kim G.J., Kim J.I. and Jin Y.S., High speed terahertz pulse imaging in the reflection geometry and image quality enhancement by digital image processing, J. Infrared and Millimeter Waves, 2008, 29(1), 79-88.

[10] Sinyukov A.M., Liu Z.W., Hor Y.L., Su K., Barat R.B., Gary D.E., Michalopoulou Z.H., Zorych I., Federici J.F. and Zimdars D., Rapid-phase modulation of terahertz radiation for high-speed terahertz imaging and spectroscopy, Opt. Lett., 2008, 33(14), 1593-1595.

[11] Jackson J.B., Labaune J., Mourou G., Duling I.N., Walker G., Bowen J. and Menu M., Terahertz pulse imaging of stratified architectural materials for cultural heritage studies, Proceedings of SPIE - The International Society for Optical Engineering, O3A: Optics for Arts, Architecture, and Archaeology III, Munich, Germany,May 25-26, 2011, 8084.

[12] Jiang T., Shen H.L., Yang X.D., Liu J.J. and Zhe Z., Target detection of THz images based on C-means of fuzzy local information, Laser Technol., 2015, 39(3), 289-294.

[13] Buades A., Coll B. and Morel J., A non-local algorithm for image denoising, IEEE-International Conference on Computer Vision and Pattern Recognition, San Diego, CA, 2005, 60-65.

[14] You Y.L. and Kaveh M., Fourth-order partial differential equations for noise removal, IEEE T. Image Process., 2000, 9(10), 1723-1730.

[15] Benhamza K., Merabti H. and Seridi H., Adaptive edge detection using ant colony, 8th International Workshop on Systems, Signal Processing and their Applications (WoSSPA), Zeralda, ALGERIA, 2013, 197-202.

[16] Pereira C., Goncalves L. and Ferreira M., Optic disc detection in color fundus images using ant colony optimization, Med. Biol. Eng. Comput., 2013, 51(3), 295-303.

[17] Dorigo M., Birattari M. and Stutzle T., Ant colony optimization-Artificial ants as a computational intelligence technique, IEEE Comput. Intell. Mag. 2006, 1(4), 28–39.

[18] Yang J.F., Zhang Y. and Yin W.T., A fast alternating direction method for TVL1-L2 signal reconstruction from partial fourier data, IEEE Journal of Selected Topics in Signal Processing, 2010, 4(2), 288-297.

[19] Wang F.Y., Wang S.Q., Hu X. and Deng C.Z.,. Compressive sensing of image reconstruction based on shearlet transform, Mechanical Engineering and Technology, AISC 125, 2012, 445-451.

[20] Donoho D.L. and Johnstone I.M., Ideal spatial adaptation via wavelet shrinkage, Biometrika, 1994, 81, 425–455.

[21] Khare A. and Tiwary U.S., Soft-thresholding for denoising of medical images - A multiresolution approach, Int. J. Wavelets Multi., 2005, 3(4), 477-496.

[22] Yang O. and Bo H., Image denoising algorithm using adaptive bayes threshold by subband based on nonsubsampled contourlet transform, 2013 Third International Conference on Intelligent System Design and Engineering Applications (ISDEA), JAN 16-18, 2013, 832-835.

[23] Dabov K., Foi A., Katkovnik V., Egiazarian K., Image denoising with block-matching and 3D filtering, Proceedings of SPIE- Conference on Image Processing - Algorithms and Systems, Neural Networks, and Machine Learning, San Jose, CA, JAN 16-18, 2006, 6064, 606414-606412.